University of Bath

Alternative formats
If you require this document in an alternative format, please contact:
openaccess@bath.ac.uk

Attenuation and focusing of ocean wave energy by a parabolic arc pontoon breakwater in a hybrid energy harvesting system

Junqing Ren[a], *Peng Jin*[a,b,*], *Yingyi Liu*[c], *Jun Zang*[b,*]

[a] College of Shipbuilding Engineering, Harbin Engineering University, Harbin 150001, China

[b] Department of Architecture & Civil Engineering, University of Bath, Bath, BA2 7AY, UK

[c] Research Institute for Applied Mechanics, Kyushu University, Kasuga 816-8580, Japan

Abstract

In the multifunctional system consisting of point absorber wave energy converters and a pontoon breakwater, the breakwater plays an essential role in attenuating waves on the lee side and amplifying waves for a better energy harvesting on the stoss side. The structure of breakwater is expectedly improved to enhance its wave attenuation and amplification at the same time. Here we present a novel parabolic arc breakwater and show that for a range of typical regular incident waves, it can attenuate more wave elevation and focus high waves in several regions in comparison to a straight breakwater. In further frequency-domain investigations, a special relatively-low frequency associated with the parabolic arc breakwater configuration is found and named as the critical frequency, closed to which splendid attenuation and focusing performance can be achieved. A systematic parametric study on the geometric factors (draft, width, and chord length) of the parabolic arc breakwater is thereafter carried out to examine their influence on the attenuation and focusing performance at the critical frequency. We find that an increase of the draft can reduce the critical frequency greatly so as to let it be within the real sea states, meanwhile slightly affecting the attenuation performance. An increase of the chord length has an uncertain but not large influence on the attenuation performance, whereas it enhances substantially the focusing performance. Simultaneously, an amplification rate up to 3.06 in two relatively-large focal areas in a prescribed deployment zone and an average attenuation rate of approximately 68% in a prescribed protection zone could be obtained in a commonly observed coastal wave.

Keywords: parabolic arc breakwater; wave energy; hybrid system; wave attenuation; wave focusing

1. Introduction

Wave energy attracts broad interest in recent years. Many wave energy converters and related hybrid energy harvesting systems have been proposed (e.g., Ref. [1]-[4]). Recently, wave energy converters were combined with breakwaters to form a system that the two kinds of devices share mutual benefits of function compatibility and cost reduction [5]. Due to the diversity of breakwaters [6] and wave energy converters [7], many systems were proposed [8]-[20] based on various integration methods. Here we restrict the scope within a promising and relatively new scenario [19][20], in which flexibly arranged point absorber wave energy converters (PAWECs) [21] are deployed in front of an easily-constructed and low-cost pontoon

---

breakwater. PAWECs, with their captured energy proportional to the square of wave height in ideal cases, take advantage of high local waves generated by the disturbance of pontoon breakwater and in return offer it protection from direct wave impact [19]. Better wave energy conversion and attenuation are desired for this hybrid system. For energy conversion, besides the optimization strategies for a single PAWEC or array [22]-[24], waves amplified by the breakwater are also a great auxiliary; on the other hand, attenuation of the system heavily relies on the breakwater [19]. In this sense, the breakwater is supposed to have a promotive amplification on the premise that its attenuation is guaranteed.

The idea of using artificial architecture to focus high waves for a better energy harvesting has long been investigated, although such approaches based on wave refraction [25]-[27] or Bragg resonance [28] were not first applied to breakwaters. One method was the so-called wave lens [30]. Flat plates or horizontal circular cylinders were assembled underwater in an overall biconvex [29], Fresnel [30], crescent [31], or other [32] planform. While passing through a wave lens, a monochromatic wave train is refracted by the sudden decrease in water depth and directed toward a pre-selected focal point. The mechanism is similar to that of its optical counterpart. An amplification factor (maximum focused surface elevation/incident wave amplitude) as high as 15 could be obtained for a particular wave frequency [32]. Despite its effectiveness, this method cannot be straightforwardly adapted for the pontoon breakwater and PAWECs hybrid system since the focal point is always on the lee side of the wave lens. However, inspired by the thought of directed refraction in the wave lens approach, a breakwater may instead use directed reflection to focus waves at certain locations on the stoss side. For this purpose, the breakwater's opening wall needs to be made to a particular shape that satisfies the focusing condition. One such breakwater was proposed in [33]. The planform contour of the opening wall is bent from a straight line to a parabola, analogous to the reflection of light by a two-dimensional concave mirror.

Many innovative methods have been proposed to improve the attenuation of a pontoon breakwater [34]-[43]. Perhaps the most straightforward way is slightly changing its geometry. As demonstrated in [44] and [45], width is a key factor. In two-dimensional (2D) cases, the transmission coefficient could be reduced through either extending the width of a single pontoon or placing multiple pontoons side by side. The latter may have a better performance for the same overall horizontal dimension [44], reflected by vast twin-pontoon designs [42]-[45]. Another way that can be regarded as increasing the horizontal dimension of a breakwater is by bending the structure to make its planform a circular arc [46] or V-shaped [47] pattern. By the Fermat principle of least time [48], this method also helps create a greater leeward shadow for the breakwater. The effectiveness of such an approach is demonstrated in a single arc [49] and double arc [50] configurations. Either the structure is concave toward the stoss side or the lee side, the attenuation effects are similarly effective [50]. While adapting the bending method, most of the cases are floating or bottom-mounted vertical plate breakwaters. Pontoon breakwaters are rarely seen.

The practical application of the pontoon breakwater and PAWECs multifunctional system is restricted by two inadequacies in the previous researches. The first is that an integrated evaluation of both attenuated

waves and amplified waves was necessary but rare. On the one hand, these two aspects were always studied in a separative manner, and concerns were mostly focused on the attenuated waves. On the other hand, studies on the integrated system are mainly concerned about interactions between the breakwater and the PAWECs in order to optimize the energy harvesting performance [19][20]. The second, partly due to the first, is that a simple way to simultaneously enhance both the attenuation and the amplification of waves was expected but absent. The exclusive improvement methods for attenuation were described in the literature in the previous paragraph. In [19] the authors reported that the presence of both a breakwater and a PAWEC was superior in attenuation to the presence of either. The latest only investigation on wave focusing using a pontoon breakwater was Ref. [33], in which attenuation was not considered. To remedy the inadequacies, we thereby propose a parabolic arc breakwater in the light of compatibility behind the method of changing the opening wall shape and the method of bending the whole structure. This concept can be generalized to other forms of breakwaters, but herein we demonstrate its effectiveness through the pontoon type. The novelty and motivation of this study are reflected as follows. The first is to establish a set of criteria, aiming at three-dimensional (3D) problems as those presented in the paper, to evaluate the overall performance of a breakwater considering simultaneously the wave attenuation and the wave focusing. The second is to demonstrate the superior performance of a parabolic arc breakwater through a comparative study. The third is to explore the influence of geometric factors (draft, width, and chord length) on the performance of a parabolic arc breakwater through a parametric study, hence providing a reference for practical applications.

The rest of the paper is structured as follows. In section 2 we validate the modeling and declare the performance criteria. In section 3 we carry out a comparative study between parabolic arc breakwaters and a straight breakwater. In section 4 we perform a parametric study on the parabolic arc breakwater dimensions. In section 5 we draw conclusions and remarks on future work.

2. Methodology and validation

2.1 Parabolic arc breakwater

The sketch of top view and side view of the proposed parabolic arc pontoon breakwater in the Cartesian coordinate system $oxyz$ is in Figure 1. The breakwater is freely floating. From the top view, the breakwater is a parabolic band with a uniform width w. It is symmetric about the x-axis and placed in a manner that the opening wall is tangent to the oyz plane at the z-axis. The curvature of the structure is determined by its focal distance f. The lateral dimension is characterized by chord length l. From the side view, the draft in calm water is denoted as d. The overall horizontal dimension is characterized by occupation width w_o. Water depth is denoted as h. The incident wave propagates in the positive x-direction with an angular frequency ω.
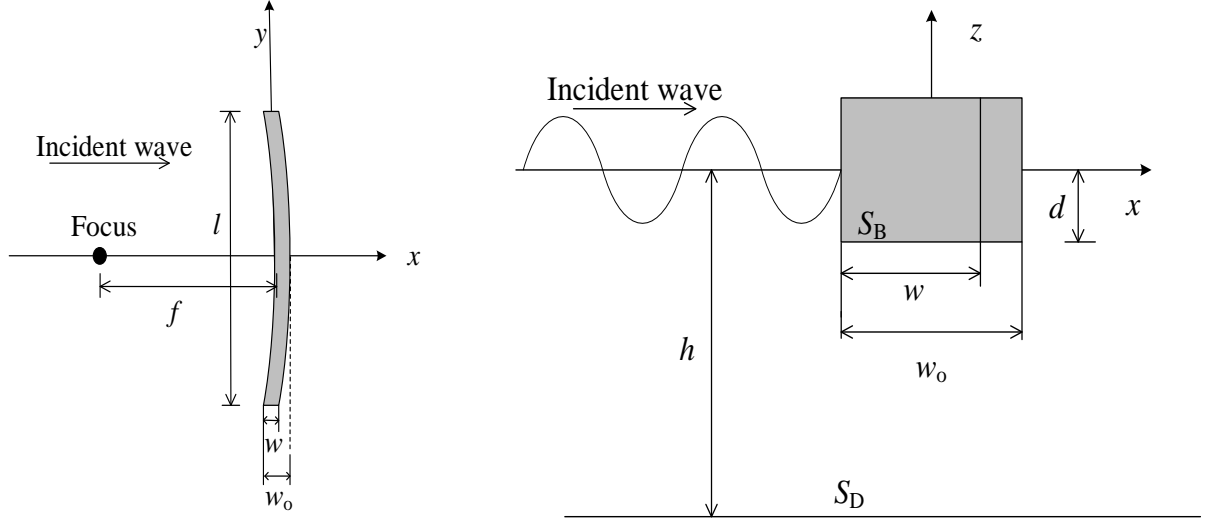
Figure 1 Sketch of the parabolic arc breakwater: top view and side view

2.2 Hydrodynamics and normalization of physical terms

Based on the potential wave theory, interactions between water waves and breakwaters are simulated by the HAMS program developed by Liu [51], incorporating an open-source package of free-surface Green function [52]. The fluid is assumed incompressible, inviscid, and irrotational, and the governing equation is the Laplace equation,

$$\nabla^2 \phi = 0 \tag{1}$$

where $\phi = \phi_0 + \phi_s + \phi_r$ is the total velocity potential. ϕ_0 is the incident potential, ϕ_s is the scattered potential, and $\phi_r = i\omega \sum_{j=1}^{6} \xi_j \phi_{rj}$ is the total radiation potential. ξ_j is the motion response and ϕ_{rj} is the radiation potential in *j*th mode oscillating with unit amplitude, respectively. The velocity potential ϕ satisfies the boundary conditions on the free surface S_F, the immersed body surface S_B, and the seabed S_D (as shown in Figure 1),

$$\left.\begin{array}{l} \frac{\partial \phi}{\partial z}|S_F = \frac{\omega^2}{g}\phi \\ \frac{\partial \phi}{\partial n}|S_B = \boldsymbol{v}_n \\ \frac{\partial \phi}{\partial z}|S_D = 0 \end{array}\right\} \tag{2}$$

where $\boldsymbol{v}_n$ is the normal component of the fluid velocity on the immersed body surface S_B. The problem can be solved in the frequency domain numerically by the Boundary Element Method using HAMS. For a planar wave, the incident potential is

$$\phi_0 = \frac{igA}{\omega} \frac{cosh[k(z+h)]}{cosh\,kh} e^{-ikx\,cos\,\beta - iky\,sin\,\beta} \tag{3}$$

where *A* is the incident wave amplitude, *g* is the acceleration of gravity, *k* is the wave number, and β is the

4

incident angle. According to Ref. **Error! Reference source not found.**, the complex surface elevation can be expressed as

$$\eta_c = \frac{\phi_0 + \phi_s}{ig/\omega} + \frac{\omega^2}{g}\sum_{j=1}^{6}\xi_j\phi_{rj} \tag{4}$$

The motion response vector $\boldsymbol{\xi}$ can be derived from the matrix form equation of motion in the frequency domain

$$[-\omega^2(\boldsymbol{m}+\boldsymbol{a}) + i\omega\boldsymbol{b} + \boldsymbol{k}_s]\boldsymbol{\xi} = \boldsymbol{F}_e \tag{5}$$

where $\boldsymbol{m}$ is the mass matrix, $\boldsymbol{a}$ the add mass matrix, $\boldsymbol{b}$ the radiation damping matrix, and $\boldsymbol{k}_s$ the hydrostatic stiffness matrix of the breakwater. $\boldsymbol{F}_e$ is the wave excitation force.

A list of major nomenclature is shown in Table 1.

Table 1 Major nomenclature

| **Breakwater**		**Water**		**Wave**	
Chord length	l	Surface elevation	η	Angular frequency	ω
Width	w	Average elevation	η_a	Period	T
Occupation width	w_o	Depth	h	Critical frequency	ω_c
Focal distance	f	Amplification factor	a		
Draft	d	Critical elevation	η_c		

2.3 Convergence test

We perform a convergence test to validate the mesh to be used in the subsequent computations. A straight pontoon breakwater with l=10 m, w=1 m, d=1 m is selected as the test model. The water depth is h=5 m. Three incident waves covering a wide range with ω=0.5, 3, and 5 rad/s are used. Three sets of mesh with a grid size of 0.1, 0.125, and 0.2 m are tested. Surface elevations on the cutting lines on the lee side of the breakwater at x=1, 10, and 19 m are displayed in Figure 2. The two sets of mesh of 0.1 m and 0.125 m match well. Hereafter the 0.125 m grid size is used in all the cases.
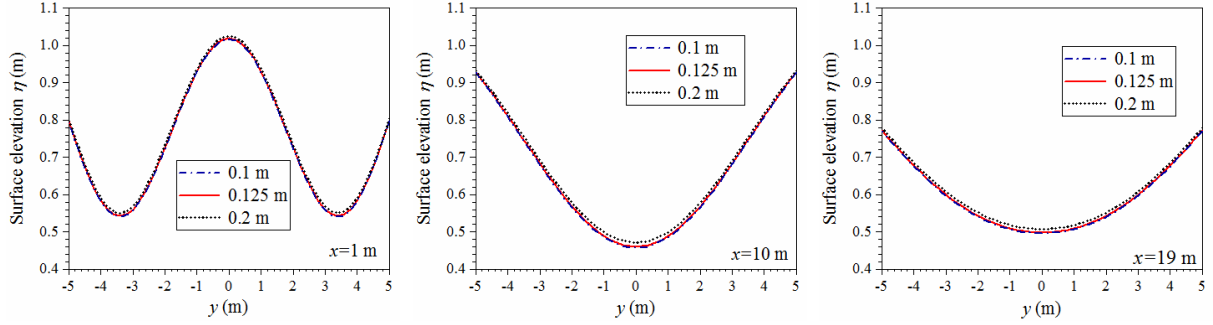
(a) ω=0.5 rad/s

(b) ω=5 rad/s
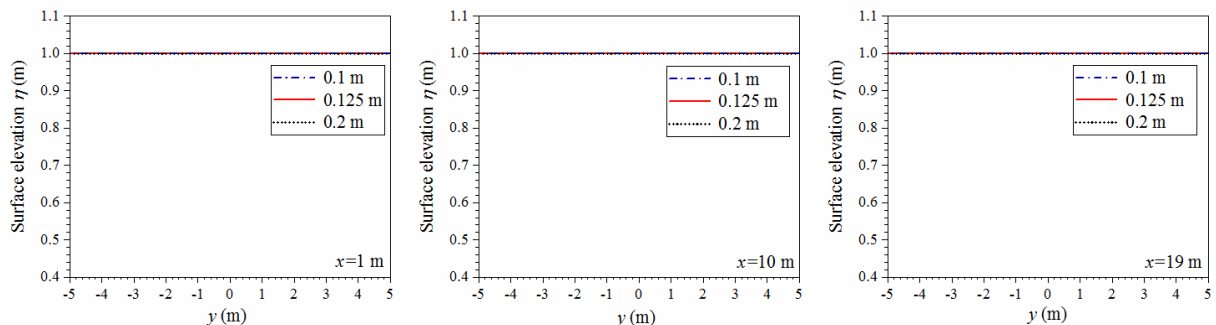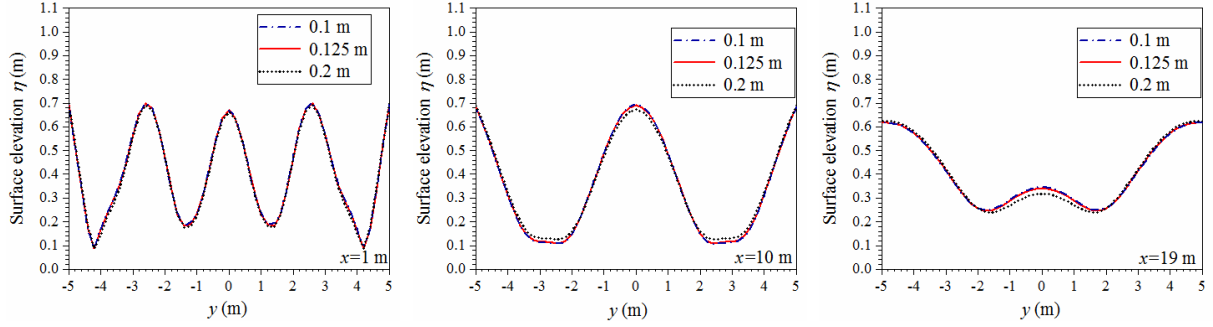
(c) ω=3 rad/s

Figure 2 Convergence test of the mesh with grid size of 0.1, 0.125, and 0.2 m, in three representative waves ω=0.1, 3, and 5 rad/s, at locations *x*=1, 10, and 19 m.

2.4 Performance criteria

The performance of a pontoon breakwater in this study is evaluated in two aspects: wave attenuation on the lee side and focusing on the stoss side. Since the main functionality of a breakwater is to reduce leeward wave elevation, attenuation is considered as the key criterion with the first priority. On the other hand, the breakwater is expected to focus high waves at some locations (possibly at the focus of the parabola) for PAWECs. High-quality focal areas are expected to have higher waves, a more regular shape (such as a square or a circle that has similar lateral and horizontal dimensions), and a larger area. Besides the criteria of attenuation and focusing, the parabolic arc breakwater should not be too curved to violate practical construction and application.

In 2D problems, wave attenuation features of a breakwater can be characterized by the transmission coefficient *T* and reflection coefficient *R*. Whereas in 3D problems, such as the present study, the concepts of *R* and *T* are no longer applicable since the surface elevation distribution in the lateral direction should not be considered as uniform (as shown in Figure 2). In such a situation, we use the surface elevation on the stoss side and the lee side to respectively describe the attenuation and focusing features. In most cases of the paper, a 50 m×*l* rectangular protection zone counted from the leeward wall center and a 50 m×*l* deployment zone counted from the opening wall center are selected in which surface elevation is measured (Figure 3). To acquire a comprehensive knowledge of attenuation, two properties throughout the protection zone are necessary: the average elevation η_a characterizing general attenuation effectiveness, and the

surface elevation η illustrating complementary details. For focusing on the deployment zone, the preference is seeking high-quality locations. In ordinary reflection by a plain obstacle, the superposition of incident and reflection waves could create waves with a maximum amplitude two times the incident amplitude. To demonstrate the superior focusing effect of parabolic arc breakwaters, areas with wave amplitude larger than 2 m and proper shape and size are marked. Associated with each focal area, the amplification factor a is also given.
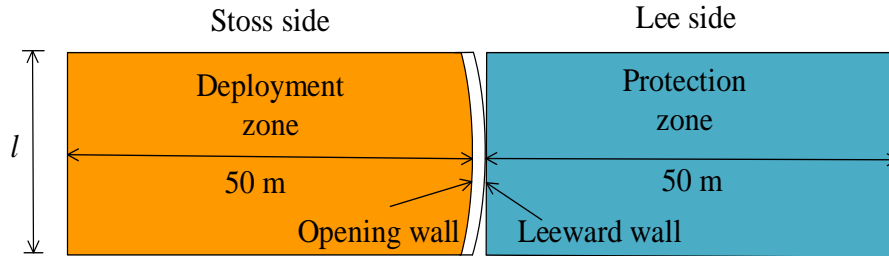
Figure 3 Protection zone and deployment zone

3. Comparative study between parabolic arc and straight breakwaters

According to the performance criteria, a comparative study is carried out to demonstrate the effectiveness of parabolic arc breakwater in wave attenuation and focusing. Seven parabolic arc breakwaters with f=10, 15, 20, 25, 30, 35, 40 m are thereby selected in comparison to a straight breakwater. It starts from f=10 m since the curvature is considered better not to be large. In all the breakwaters, the chord length is l=20 m, the width is w=1 m, and the draft is d=1 m. The water depth is h=5 m. Nine groups of incident regular waves with an angular frequency ω ranging from ω=1 to 5 rad/s with an increment of 0.5 rad/s are used to check the performance of breakwaters in a different wave environment.

3.1 Attenuation

The comparative results of the average elevation η_a for each wave are displayed in Figure 4. For ω=1, 1.5, and 2 rad/s, η_a around all the eight breakwaters keeps close to 1 m. Either a parabolic or straight breakwater is almost useless. For ω=2.5 rad/s, the breakwaters begin to work but are similarly ineffective with a η_a about 0.9 m. The f=10 m parabolic arc breakwater is a little better than the rest. For ω=3, 3.5, 4, 4.5, and 5 rad/s, η_a of all the breakwaters drops a lot. It is evident that η_a of the seven parabolic arc breakwaters is lower than that of the straight breakwater. To sum up, in our selected cases, the parabolic arc breakwaters are as good as or better than the straight breakwater, especially in the high-frequency waves. Also, for $\omega \geq 3$ rad/s, attenuation is stronger as the focal distance f increases (the straight breakwater may be regarded as a parabolic arc breakwater with f=+∞). The f=10 m parabolic arc breakwater has an overall best attenuation at an average level.

Next, we look closely to see how better the attenuation of the f=10 m parabolic arc breakwater could be in contrast to that of the straight breakwater in the high-frequency waves. By calculating the ratio of

difference $(\eta_{a|straight}-\eta_{a|f=10\,m})/\eta_{a|f=10\,m}$, we have for ω=3, 3.5, 4, 4.5, and 5 rad/s, η_a of the f=10 m parabolic arc breakwater is less than that of the straight breakwater by respective ratios of 44.23%, 55.32%, 54.17%, 51.55%, and 30.26%.
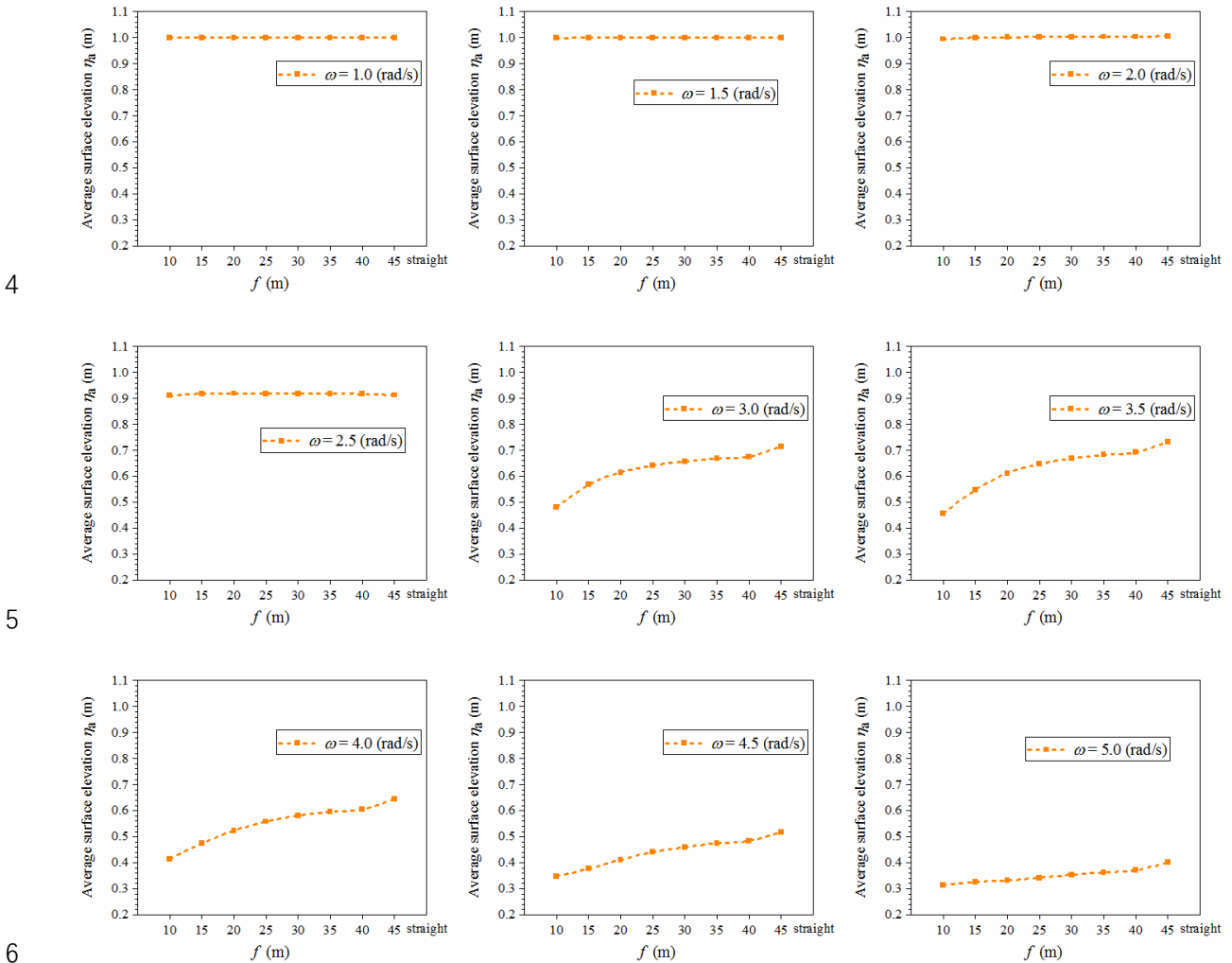
Figure 4 Trends of average elevation η_a in protection zone, with respect to seven parabolic arc breakwaters with f=10, 15, 20, 25, 30, 35, 40 m and a straight breakwater. w=1 m. d=1 m. ω=1 to 5 rad/s with an increment of 0.5 rad/s.
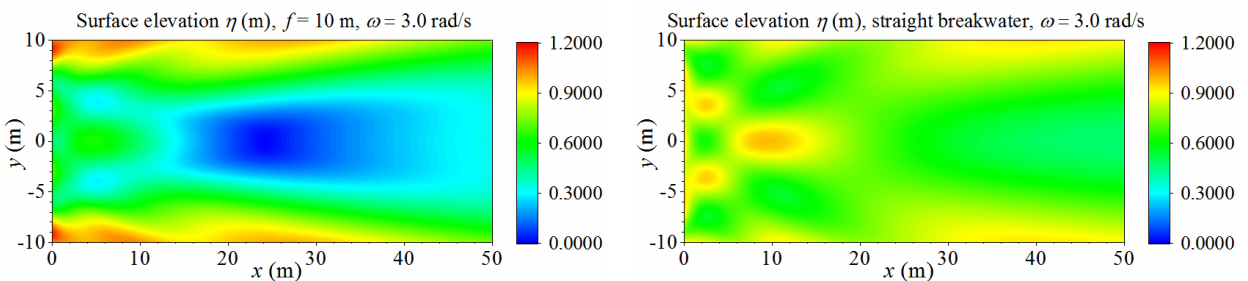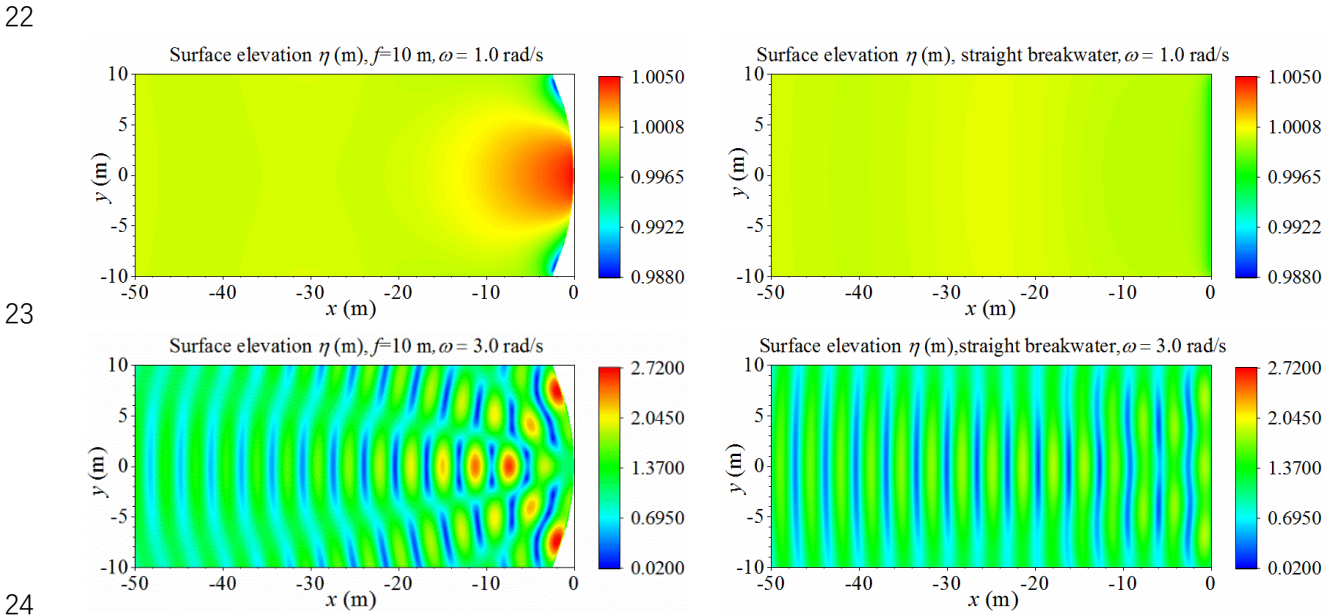

Figure 5 Surface elevation η in the protection zone of the f=10 m parabolic arc breakwater (left) and straight breakwaters (right), where w=1 m, d=1 m, l=20 m, ω=3 rad/s.

Surface elevation η distribution is illustrated as complementary details for the comparison of attenuation

8

between the f=10 m parabolic arc breakwater and the straight breakwater. Here we take the ω=3 rad/s case as an example (Figure 5). The most distinctive character of the leeward wave field of the parabolic arc breakwater is the roughly stratified pattern in y-direction: narrow high elevation layer (yellow and red) on the boundaries, low elevation layer (mainly blue) in the central part, and the medium elevation layer (green) in between. No high elevation spot is mixed in the low and medium elevation areas as that in the pattern of the straight breakwater. Laterally, from outer to inner of the protection zone, wave motion decreases. In a large area (mainly blue) in the central part, wave motion could be quite faint. According to the Fermat principle of least time [48], the convex leeward wall is able to direct waves outward the central zone, reducing interactions between waves and preventing focusing. This may explain the distribution pattern and the better attenuation of the parabolic arc breakwater.

3.2 Focusing

To examine the wave focusing performance of the f=10 m parabolic arc breakwater and the straight breakwater, the distribution of η in three representative waves (from low to high, ω=1, 3, and 5 rad/s) are displayed in Figure 6. For each wave in this case and hereafter, the maximum elevation in the entire deployment zone is used as the upper bound in the rainbow ribbon on the right side of the pictures. The lower bounds are chosen accordingly for the best clarity. In all three waves, the straight breakwater, in general, shows a wave field with a periodical strip pattern, revealing little apparent focusing. Whereas the parabolic arc breakwater is able to focus higher waves in some locations (red spots), the focusing strength is varying in different waves. High focusing happens in high-frequency waves. As we see in ω=5 rad/s, a could be 4.74. The incident wave is amplified by nearly five times at the focus of the parabola.
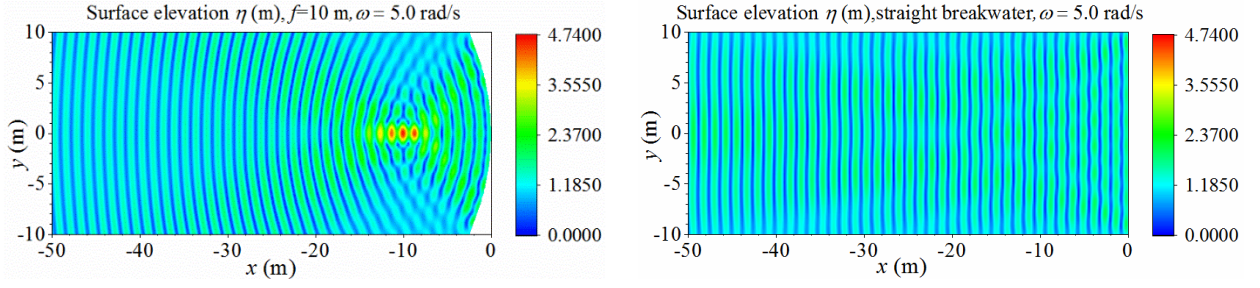
Figure 6 Surface elevation η in the deployment zone of the f=10 m parabolic arc breakwater (left column) and straight breakwater (right column), where w=1 m, d=1 m, l=20 m, ω=1, 3, 5 rad/s.

4. Parametric study on the dimensions of the parabolic arc breakwater

In the previous section, we demonstrate the performance of a representative f=10 m parabolic arc breakwater in wave attenuation and focusing. In this part, we will study the influence of its draft, width, and chord length on the performance. The water depth is h=5 m. Incident waves are from 0.5 to 5 rad/s with an increment of 0.01 rad/s.

4.1 Draft

Here the width and chord length are kept fixed as w=1 m and l=20 m. A series of draft d=1, 1.5, 2, 2.5, 3 m are used.

The results of η_a in the protection zone of the five breakwaters are in Figure 7a. We see that attenuation in the five cases shows similar general trends in the frequency domain. The most interesting finding is the existence of sharp local minima. On this point and in the narrow adjacent range around it, relatively low-frequency waves can be effectively attenuated. Herein we would name this particular frequency as the critical frequency by denoting it as ω_c. The corresponding local minima of η_a is named as the critical elevation by denoting it as η_c. The breakwater can be potentially tuned to make its critical frequency match the local wave frequency in order to obtain a satisfying attenuation effect.
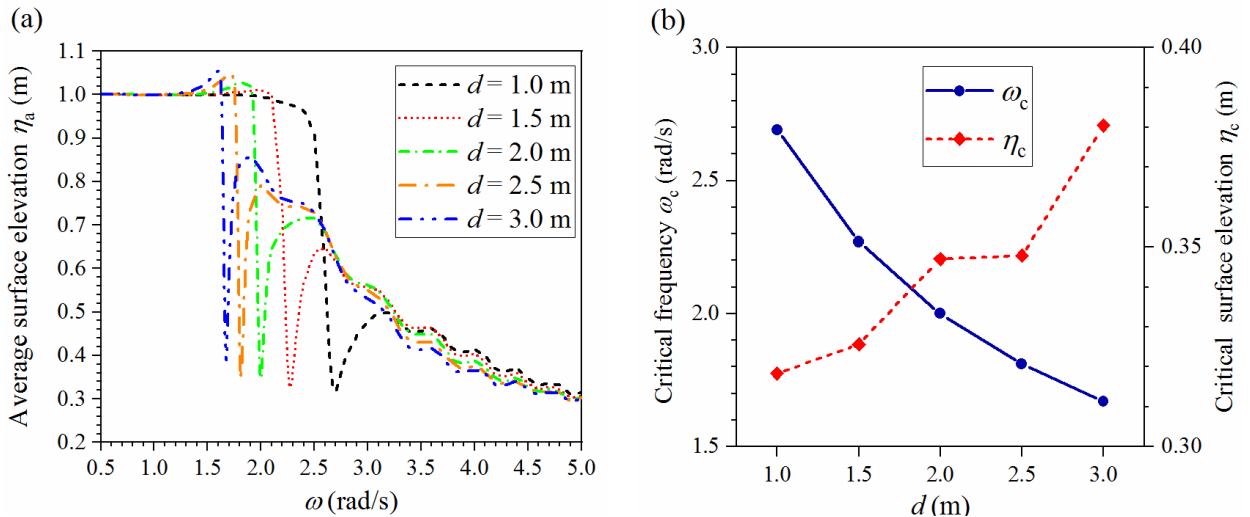
Figure 7   a. Average elevation η_a in the frequency domain in the protection zone of the f=10 m parabolic arc breakwaters. b. Trend of critical frequency ω_c and critical elevation η_c with respect to d, where w=1 m, l=20 m, d=1, 1.5, 2, 2.5, 3 m.

Results of ω_c and η_c for the different drafts are displayed in Figure 7b. As d increases from 1 to 3 m, ω_c decreases a lot from 2.69 to 1.67 rad/s, η_c increases not much from 0.315 to 0.38 m. ω_c is quite sensitive to the change of d, whereas η_c is not. It indicates that the critical frequency of the breakwater can be effectively reduced by increasing the draft, without loss of much attenuation ability. But such an approach may have some latent limits. First, although the critical elevation does not increase much, it still increases (about 20%), and the attenuation worsens. Other methods, such as installing extended porous plates [39] on the bottom of the leeward wall, may be an alleviation. Second, from Figure 7b one could observe that the decreasing of the critical frequency is slower as the draft increases. Using this method to reduce the critical frequency could be harder for a large draft. Third, as the draft increases, the pattern around the critical point becomes sharper. The effective band is narrower, and the attenuation performance is more sensitive to a varying incident wave frequency around the critical point.

In the five critical frequencies, ω_c=1.81 rad/s for d=2.5 m and ω_c=1.67 rad/s for d=3 m are in the range from 1 to 2 rad/s, which is commonly observed in some coastal areas in southwest England [54] and Shandong, China [4]. Here we take the latter case with lower ω_c for further investigation. The results of η in the deployment zone and protection zone under the critical condition are shown in Figure 8. The focal areas with a>2 are circled by black lines, and the amplification factor a in the large one (maximum surface elevation in the circled area/incident wave amplitude) is shown. For attenuation, the low elevation zone (blue) appears a butterfly shape and is mainly in the region closed to the leeward wall. The breakwater could be properly placed to cover targeted infrastructures in this area. The elevation is mostly around 0.5 m in the rest of the area, which is also a reasonable shelter. On the stoss side, the breakwater mainly focuses a large elliptic a>2 area with a=2.43. Between -20 m<x<-10 m, another a>2 area may be discarded since it is small.
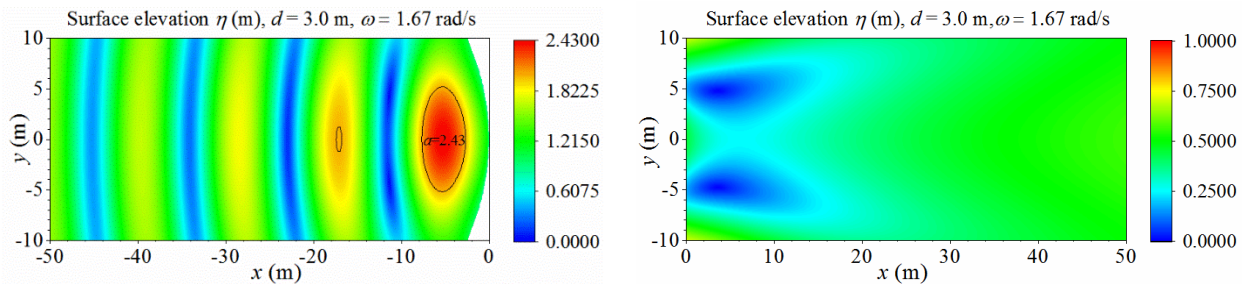
Figure 8 Surface elevation η in the deployment zone (left) and protection zone (right) behind the f=10 m parabolic arc breakwater in the d=3 m case, where w=1 m, l=20 m. Focal areas with a>2 are circled by the solid line. Amplification factor a in the large focal area is given.

4.2 Width

Here the draft is d=3 m, and the chord length is l=20 m. A series of width w=1, 1.5, 2, 2.5, 3 m are used.

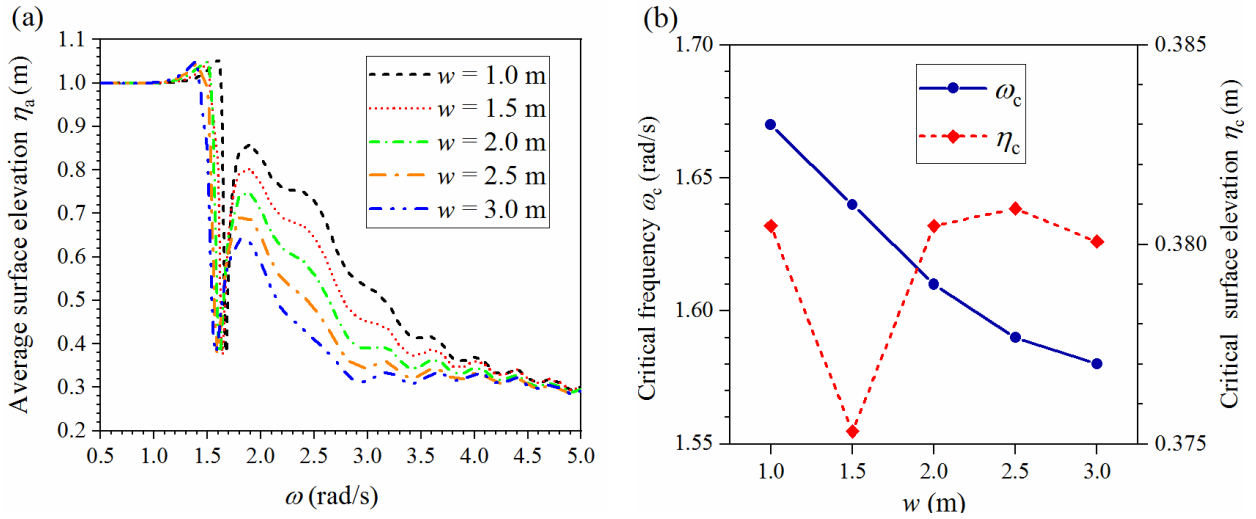**Figure 9** a. Average elevation η_a in the frequency domain in the protection zone of the f=10 m parabolic arc breakwaters. b. The trend of critical frequency ω_c and critical elevation η_c with respect to w, where d=1 m, l=20 m, w=1, 1.5, 2, 2.5, 3 m.

The results of η_a in the frequency domain are in Figure 9a. As w increases, η_a after ω_c is greatly reduced, but η_a before ω_c is hardly affected. Also, the pattern around the critical point is less sharp. ω_c and η_c for different width are displayed in Figure 9b. ω_c drops not much from 1.67 rad/s for ω=1 to 1.58 rad/s for w=3 m, whereas η_c has only tiny fluctuation around 0.38 m. From the above results, the critical frequency could be reduced by increasing its width, but the method is not as effective as an increasing draft (Figure 7b). The decreasing of critical frequency also shows a slowdown as the width increases. For attenuation under the critical condition, increasing width has a negligible effort, but the effective band around the critical point becomes wider, making the attenuation less sensitive to a varying incident wave frequency. Besides, an increased width is quite effective in suppressing high-frequency waves.
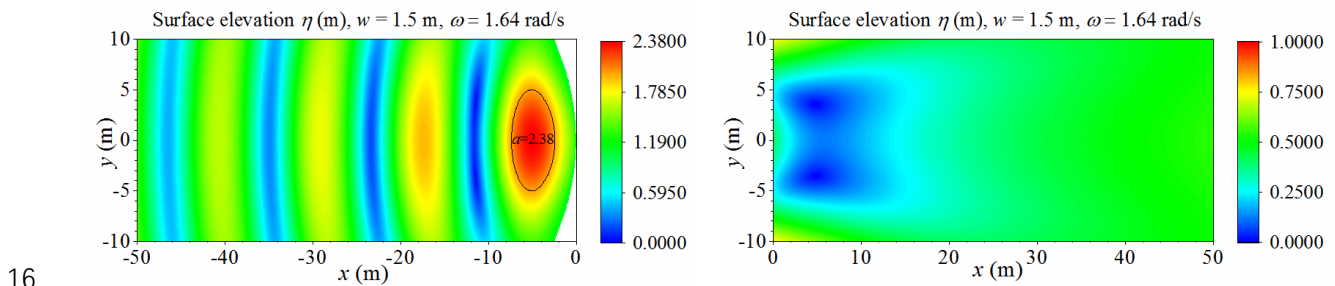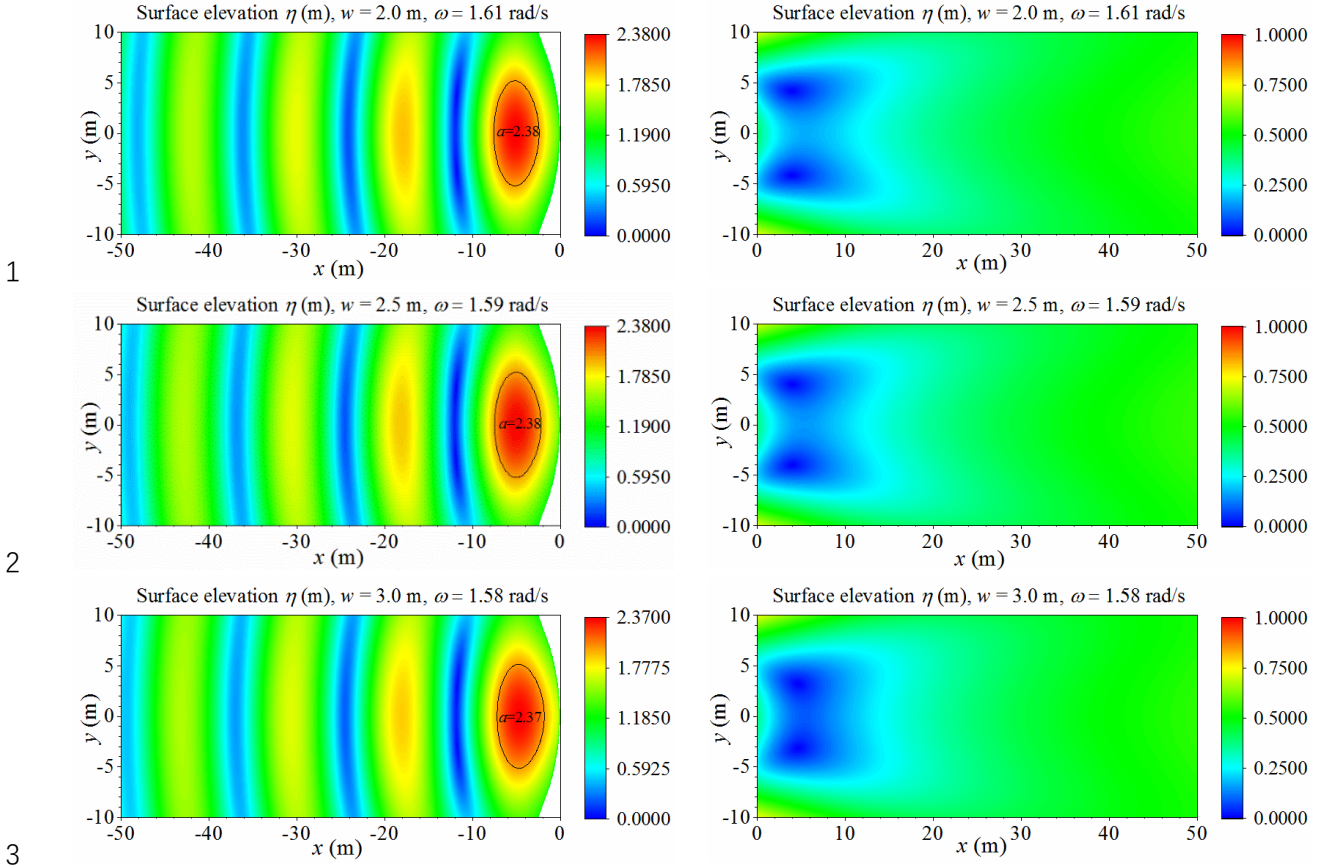
Figure 10 Surface elevation η in the deployment zone (left) and protection zone (right) behind the f=10 m parabolic arc breakwater for w=1.5, 2, 2.5, 3 m, where d=1 m, l=20 m. Focal areas with a>2 are circled by solid line. Amplification factor a in each large focal area is given.

The distribution of η in the deployment zone and protection zone of the w=1.5, 2, 2.5, 3 m breakwaters under the critical condition are in Figure 10. Together with Figure 8, we find that changing width has a very limited influence on the shape and amplification factor a of the high elevation area. The distribution in the protection zone is also not affected much.

4.3 Chord length
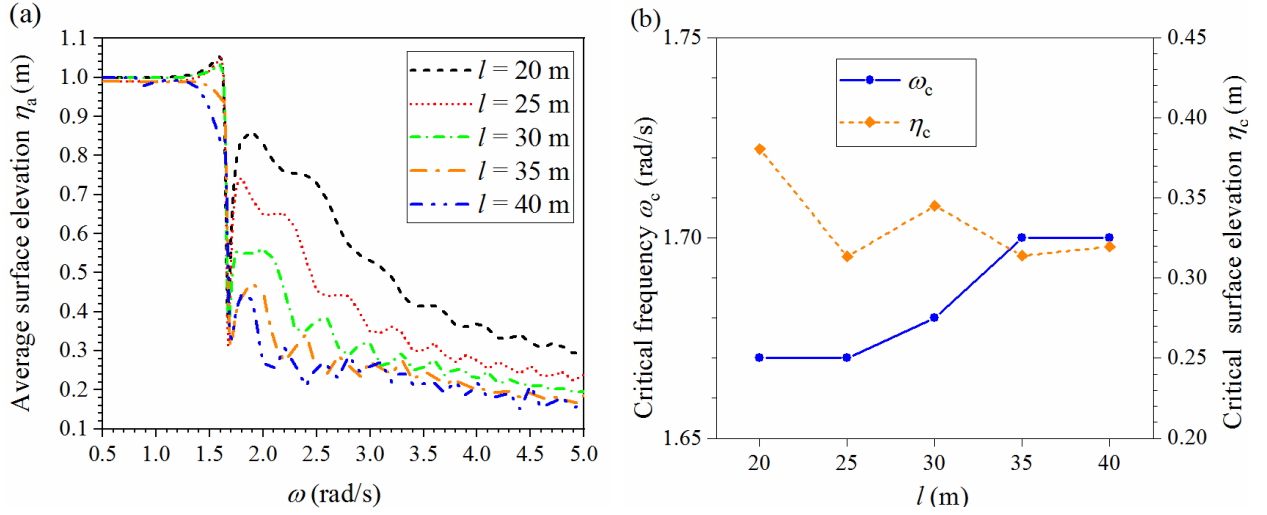
In this part, as we increase the chord length of the breakwater, we keep the targeted protection zone invariant as a 50 m×20 m area, as in the previous sections. The deployment zone is changing with the breakwater as a 50 m×l area. The draft is d=3 m, and the width is w=1 m. Chord length l=20, 25, 30, 35, 40 m are used.

Figure 11 a. Average elevation η_a in the frequency domain in the protection zone of the f=10 m parabolic arc breakwaters. b. The trend of critical frequency ω_c and critical elevation η_c with respect to l, where w=1 m, d=1 m, l=20, 25, 30, 35, 40 m.

In Figure 11a, we see that as l increases, η_a after the critical point is greatly reduced. This method is more effective than increasing the width (Figure 9a) in suppressing waves beyond the critical frequency. The pattern around the critical point becomes less sharp; attenuation is less sensitive to a varying spectrum. In Figure 11b, ω_c slightly increases from 1.67 rad/s for l=20 m to 1.7 rad/s for l=40 m, whereas η_c fluctuates in a range from 0.31 to 0.38 m. Increasing chord length has a little negative effect on the reduction of critical frequency and a relatively random effect on attenuation under the critical condition.

The distribution of η in the deployment zone and protection zone (bounded by dashed lines) of the l=25, 30, 35, 40 m breakwaters under the critical condition are in Figure 12. Amplification factor a in each large focal area is marked. Together with that in Figure 8, the pattern in the protection zone in the five cases are similar. The low elevation region is closely behind the leeward wall. In the deployment zone, as the chord length increases, high focal areas gradually move from the central part to the sides. As the attenuation and focusing are not changing monotonically with the chord length, the five cases need to be treated accordingly. First, we should discard the l=30 m case. With an increase in the construction material, higher critical frequency and elevation, lower amplification factors, and not larger focal areas, it has little advantage comparing with the l=25 m case. The l=25 m case is quite good, the critical frequency and elevation are among the lowest, and the two focal areas are relatively large with reasonable amplification factors. The l=35 and 40 m cases are similar in attenuation, and they both mainly have two symmetric high focal areas. The l=40 m case has a bit advantage in the amplification factor and size of the focal area. The low and small focal areas could be used for PAWECs, but the high and large focal areas are much better.

14
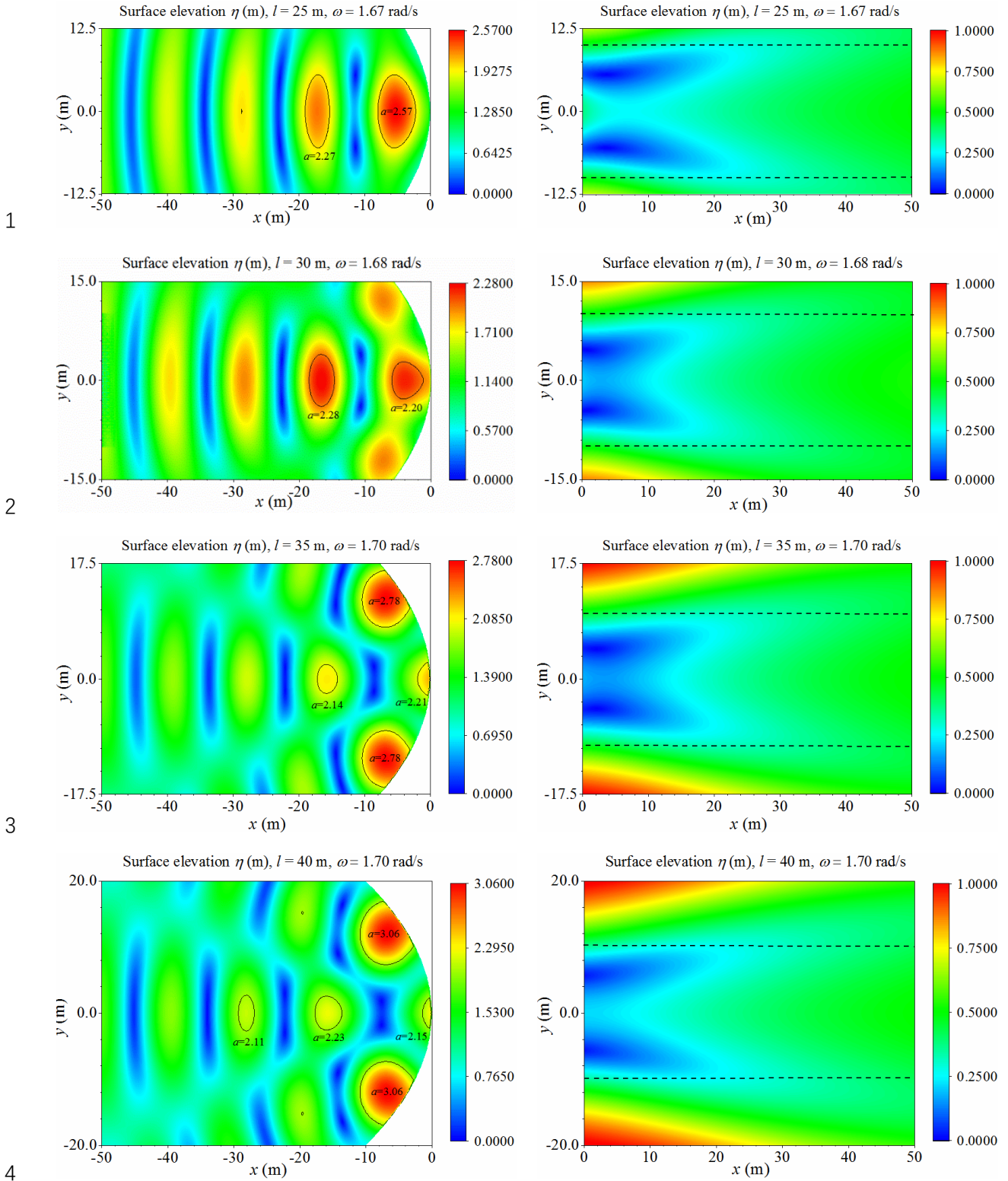
Figure 12 Surface elevation η in the deployment zone (left column) and protection zone (right column) behind the f=10 parabolic arc breakwater for l=25, 30, 35, 40 m, where w=1 m, d=1 m. Protection zones are bounded by dashed lines. Focal areas with a>2 are circled by the solid line. Amplification factor a in each large focal area is given.

Except for the l=30 m case, attenuation, especially in high-frequency waves, and focusing are generally improved as we increase chord length. However, we should also consider the geometry of the breakwater.

The occupation width (see Figure 1) is $w_o=w+l^2/16f$. For fixed f and w, w_o-w is proportional to l^2. As l increases, w_o increases in an approximately quadratic speed. If the chord length is made very large, the occupation width and total length (the length of the parabola) will be much larger, leading to an abnormal shape and excessive use of construction material. A compromise between the performance and the shape has to be made.

5. Conclusion

The hybrid system of wave energy converters and breakwaters has become an active research area. This study proposes a novel parabolic arc pontoon breakwater to improve attenuation performance and focus high waves for PAWECs. The adaption of the code is validated by a convergence test. Surface elevation in the development zone and protection zone and amplification factor are used as the main criteria for the assessment of attenuation and focusing performance. Through a comparative study between the parabolic arc and straight breakwaters in nine different waves and a parametric study on the f=10 m parabolic arc breakwater in a wide frequency range, the major remarks are concluded as follows:

1. A parabolic arc breakwater is as good as or better than a straight breakwater in attenuation, especially in high-frequency waves. The f=10 m parabolic arc breakwater is able to focus high waves at certain locations, whereas the straight breakwater is not.

2. A relatively-low critical frequency is found in the narrow band around which the parabolic arc breakwater has excellent attenuation and focusing performance. The strategy of the breakwater design could be formulated so as to match the critical frequency with the peak frequency at the operation sites.

3. Increasing draft of the parabolic arc breakwater is the most effective way to reduce the critical frequency, whereas slightly rise the corresponding critical elevation. Increasing width can slightly reduce the critical frequency and has a small influence on the critical elevation. Increasing chord length raises the critical frequency a little and has an uncertain but not large influence on the critical elevation. While doing so, the balance between the performance and shape of the parabolic arc breakwater should also be considered. A combination of the methods of varying dimensions and others is possible to tune the breakwater to be effective in a prescribed wave environment. Based on the present study, a breakwater is found to be capable of attenuating approximate 68% of the elevation as well as to focus two large areas with an amplified factor of 3.06 in a 3.7s wave, which is commonly observed in some coastal areas in southwest England and Shandong Province, China.

Future work will explore in detail the general design criteria of a parabolic arc breakwater considering the wave attenuation and focusing performance based on the findings of the present study, which will be investigated in a later stage.

1 Acknowledgement

4 Appendix

5 The Position of center of gravity, mass, and moment of inertia of the floating breakwaters used in this
6 study are listed in Table 2. The body-fixed coordinate system *OXYZ* is located at the center of gravity of a
7 breakwater. The deployment of the breakwater is shown in Figure 1.

8 **Table 2** Position of center of gravity, mass, and moment of inertia of the floating breakwaters

l=20 m, *w*=1 m, *d*=1 m					
f (m)	Position of center of gravity in the inertia coordinate system (m)	Breakwater mass (Kg)	Moment of inertia (Kg·m²)		
			I_{XX}	I_{YY}	I_{ZZ}
10	(-0.333, 0, 0)	2.050E+04	7.510E+05	2.803E+04	7.568E+05
15	(-0.056, 0, 0)	2.050E+04	7.444E+05	2.083E+04	7.428E+05
20	(0.083, 0, 0)	2.050E+04	7.419E+05	1.833 E+04	7.378E+05
25	(0.167, 0, 0)	2.050E+04	7.417E+05	1.717 E+04	7.355E+05
30	(0.222, 0, 0)	2.050E+04	7.401E+05	1.655 E+04	7.342E+05
35	(0.262, 0, 0)	2.050E+04	7.397E+05	1.617 E+04	7.334E+05
40	(0.292, 0, 0)	2.050E+04	7.395E+05	1.593E+04	7.329E+05
straight	(0.5, 0, 0)	2.050E+04	7.386E+05	1.513E+04	7.313E+05
f =10 m, *l*=20 m, *w*=1 m					
d (m)	Position of center of gravity in the inertia coordinate system (m)	Breakwater mass (Kg)	Moment of inertia (Kg·m²)		
			I_{XX}	I_{YY}	I_{ZZ}
1.5	(-0.333, 0, 0)	3.075E+04	1.154E+06	5.988E+04	1.146E+06
2	(-0.333, 0, 0)	4.100E+04	1.576E+06	1.103E+05	1.536E+06
2.5	(-0.333, 0, 0)	5.125E+04	2.023E+06	1.843E+05	1.927E+06
3	(-0.333, 0, 0)	6.150E+04	2.498E+06	2.872E+05	2.319E+06
f =10 m, *l*=20 m, *d*=3 m					
w (m)	Position of center of gravity in the inertia coordinate system (m)	Breakwater mass (Kg)	Moment of inertia (Kg·m²)		
			I_{XX}	I_{YY}	I_{ZZ}
1.5	(-0.083, 0, 0)	9.255E+04	3.862E+06	4.850E+05	3.591E+06
2	(0.167, 0, 0)	1.230E+05	5.280E+06	7.226E+05	4.931E+06
2.5	(0.417, 0, 0)	1.538E+05	6.742E+06	1.003E+06	6.336E+06
3	(0.667, 0, 0)	1.845E+05	8.238E+06	1.330E+06	7.806E+06
f =10 m, *d*=3 m, *w*=1 m					
l (m)	Position of center of gravity in the inertia coordinate system (m)	Breakwater mass (Kg)	Moment of inertia (Kg·m²)		
			I_{XX}	I_{YY}	I_{ZZ}
25	(-0.802, 0, 0)	7.688E+04	4.700E+06	4.284E+05	4.546E+06
30	(-1.375, 0, 0)	9.225E+04	7.989E+06	6.646E+05	7.957E+06
35	(-2.052, 0, 0)	1.076E+05	1.262E+07	1.065E+06	1.287E+07
40	(-2.833, 0, 0)	1.230E+05	1.885E+07	1.725E+06	1.966E+07

9 Reference

[1] Ning, D. Z., Wang, R. Q., Zou, Q. P., & Teng, B. (2016). An experimental investigation of hydrodynamics of a fixed OWC Wave Energy Converter. Applied Energy, 168, 636-648.

[2] Perez-Collazo, C., Greaves, D., & Iglesias, G. (2018). Hydrodynamic response of the WEC sub-system of a novel hybrid wind-wave energy converter. Energy Conversion and Management, 171, 307-325.

[3] Elhanafi, A., Macfarlane, G., & Ning, D. (2018). Hydrodynamic performance of single–chamber and dual–chamber offshore–stationary Oscillating Water Column devices using CFD. Applied Energy, 228, 82-96.

[4] Hu, J., Zhou, B., Vogel, C., Liu, P., Willden, R., Sun, K., ... & Collu, M. (2020). Optimal design and performance analysis of a hybrid system combing a floating wind platform and wave energy converters. Applied Energy.

[5] Mustapa, M. A., Yaakob, O. B., Ahmed, Y. M., Rheem, C. K., Koh, K. K., & Adnan, F. A. (2017). Wave energy device and breakwater integration: A review. *Renewable and Sustainable Energy Reviews*, *77*, 43-58.

[6] Dai, J., Wang, C. M., Utsunomiya, T., & Duan, W. (2018). Review of recent research and developments on floating breakwaters. *Ocean Engineering*, *158*, 132-151.

[7] Babarit, A. (2017). *Ocean wave energy conversion: resource, technologies and performance*. Elsevier.

[8] Xu, C., & Huang, Z. (2018). A dual-functional wave-power plant for wave-energy extraction and shore protection: A wave-flume study. *Applied Energy*, *229*, 963-976.

[9] Zheng, S., & Zhang, Y. (2018). Analytical study on wave power extraction from a hybrid wave energy converter. *Ocean Engineering*, *165*, 252-263.

[10] Chen, B., Bruce, T., Greated, C. A., & Kang, H. (2017). Dynamic behavior of a wave power buoy with interior on-board linear generator. *Ocean Engineering*, *129*, 374-381.

[11] Krishnendu, P., & Balaji, R. (2020). Hydrodynamic performance analysis of an integrated wave energy absorption system. *Ocean Engineering*, *195*, 106499.

[12] Zhang, H., Zhou, B., Vogel, C., Willden, R., Zang, J., & Zhang, L. (2020). Hydrodynamic performance of a floating breakwater as an oscillating-buoy type wave energy converter. *Applied Energy*, *257*, 113996.

[13] Zhang, X., Zeng, Q., & Liu, Z. (2019). Hydrodynamic Performance of Rectangular Heaving Buoys for an Integrated Floating Breakwater. *Journal of Marine Science and Engineering*, *7*(8), 239.

[14] Peng, W., Fan, Y., & Zhang, J. (2018). Numerical Study on Optimization of the Float in a Shoreline Wave Energy Converter. *Journal of Coastal Research*, *85*(sp1), 1296-1300.

[15] Madhi, F., & Yeung, R. W. (2018). On survivability of asymmetric wave-energy converters in extreme waves. *Renewable Energy*, *119*, 891-909.

[16] De Almeida, J. L. (2017). REEFS: An artificial reef for wave energy harnessing and shore protection– A new concept towards multipurpose sustainable solutions. *Renewable energy*, *114*, 817-829.

[17] Di Lauro, E., Lara, J. L., Maza, M., Losada, I. J., Contestabile, P., & Vicinanza, D. (2019). Stability analysis of a non-conventional breakwater for wave energy conversion. *Coastal Engineering*, *145*, 36-52.

[18] Vicinanza, D., & Frigaard, P. (2008). Wave pressure acting on a seawave slot-cone generator. *Coastal Engineering*, *55*(6), 553-568.

[19] Zhang, H., Zhou, B., Vogel, C., Willden, R., Zang, J., & Geng, J. (2020). Hydrodynamic performance of a dual-floater hybrid system combining a floating breakwater and an oscillating-buoy type wave

1   energy converter. *Applied Energy*, *259*, 114212.

2   [20] Reabroy, R., Zheng, X., Zhang, L., Zang, J., Yuan, Z., Liu, M., ... & Tiaple, Y. (2019). Hydrodynamic
3   response and power efficiency analysis of heaving wave energy converter integrated with
4   breakwater. *Energy Conversion and Management*, *195*, 1174-1186.

5   [21] Zheng, S., Zhang, Y., & Iglesias, G. (2020). Concept and performance of a novel wave energy
6   converter: Variable Aperture Point-Absorber (VAPA). Renewable Energy, 153, 681-700.

7   [22] Bachynski, E. E., Young, Y. L., & Yeung, R. W. (2012). Analysis and optimization of a tethered wave
8   energy converter in irregular waves. *Renewable energy*, *48*, 133-145.

9   [23] Jin, P., Zhou, B., Göteman, M., Chen, Z., & Zhang, L. (2019). Performance optimization of a coaxial-
10   cylinder wave energy converter. *Energy*, *174*, 450-459.

11   [24] Noad, I. F., & Porter, R. (2015). Optimisation of arrays of flap-type oscillating wave surge
12   converters. *Applied Ocean Research*, *50*, 237-253.

13   [25] Mehlum, E., & Stamnes, J. (1978). On the focusing of ocean swells and its significance in power
14   production. *Cent. Inst. for Indust. Res., Blindern, Oslo, SI Rep*, *77*, 01-38.

15   [26] Hu, X., & Chan, C. T. (2005). Refraction of water waves by periodic cylinder arrays. *Physical review*
16   *letters*, *95*(15), 154501.

17   [27] Griffiths, L. S., & Porter, R. (2012). Focusing of surface waves by variable bathymetry. *Applied Ocean*
18   *Research*, *34*, 150-163.

19   [28] Elandt, R. B., Shakeri, M., & Alam, M. R. (2014). Surface gravity-wave lensing. *Physical Review*
20   *E*, *89*(2), 023012.

21   [29] Murashige, S., & Kinoshita, T. (1992). An ideal ocean wave focusing lens and its shape. *Applied ocean*
22   *research*, *14*(5), 275-290.

23   [30] Stamnes, J. J., Løvhaugen, O., Spjelkavik, B., Mei, C. C., Lo, E., & Yue, D. K. (1983). Nonlinear
24   focusing of surface waves by a lens–theory and experiment. *Journal of Fluid Mechanics*, *135*, 71-94.

25   [31] Li, C. Y., Shih, R. S., & Weng, W. K. (2020). Investigation of Ocean-Wave-Focusing Characteristics
26   Induced by a Submerged Crescent-Shaped Plate for Long-Crested Waves. *Water*, *12*(2), 509.

27   [32] Newman, J. N. (2015). Amplification of waves by submerged plates. In *30th International Workshop*
28   *on Water Waves and Floating Bodies (IWWWFB), Bristol, UK* (pp. 153-156).

29   [33] Zhang, C., & Ning, D. (2019). Hydrodynamic study of a novel breakwater with parabolic openings for
30   wave energy harvest. *Ocean Engineering*, *182*, 540-551.

31   [34] Liu, Z., Wang, Y., Wang, W., & Hua, X. (2019). Numerical modeling and optimization of a winged
32   box-type floating breakwater by Smoothed Particle Hydrodynamics. *Ocean Engineering*, *188*, 106246.

33   [35] Zhang, X. S., Ma, S., & Duan, W. Y. (2018). A new L type floating breakwater derived from vortex
34   dissipation simulation. *Ocean Engineering*, *164*, 455-464.

35   [36] Christensen, E. D., Bingham, H. B., Friis, A. P. S., Larsen, A. K., & Jensen, K. L. (2018). An
36   experimental and numerical study of floating breakwaters. *Coastal engineering*, *137*, 43-58.

37   [37] He, F., Huang, Z., & Law, A. W. K. (2013). An experimental study of a floating breakwater with
38   asymmetric pneumatic chambers for wave energy extraction. *Applied energy*, *106*, 222-231.

39   [38] Diamantoulaki, I., & Angelides, D. C. (2010). Analysis of performance of hinged floating
40   breakwaters. *Engineering Structures*, *32*(8), 2407-2423.

[39] Koutandos, E. V., & Prinos, P. E. (2011). Hydrodynamic characteristics of semi-immersed breakwater with an attached porous plate. *Ocean Engineering*, *38*(1), 34-48.

[40] Uzaki, K. I., Ikehata, Y., & Matsunaga, N. (2011). Performance of the wave energy dissipation of a floating breakwater with truss structures and the quantification of transmission coefficients. *Journal of Coastal Research*, *27*(4), 687-697.

[41] Singla, S., Behera, H., Martha, S. C., & Sahoo, T. (2019). Scattering of obliquely incident water waves by a surface-piercing porous box. *Ocean Engineering*, *193*, 106577.

[42] Ji, C. Y., Chen, X., Cui, J., Gaidai, O., & Incecik, A. (2016). Experimental study on configuration optimization of floating breakwaters. Ocean Engineering, 117, 302-310.

[43] Koo, W. (2009). Nonlinear time–domain analysis of motion-restrained pneumatic floating breakwater. *Ocean Engineering*, *36*(9-10), 723-731.

[44] Williams, A. N., Lee, H. S., & Huang, Z. (2000). Floating pontoon breakwaters. *Ocean Engineering*, *27*(3), 221-240.

[45] Dong, G. H., Zheng, Y. N., Li, Y. C., Teng, B., Guan, C. T., & Lin, D. F. (2008). Experiments on wave transmission coefficients of floating breakwaters. *Ocean Engineering*, *35*(8-9), 931-938.

[46] Duan, J. H., Cheng, J. S., Wang, J. P., & Wang, J. Q. (2012). Wave diffraction on arc-shaped floating perforated breakwaters. *China Ocean Engineering*, *26*(2), 305-316.

[47] Chang, K. H., Tsaur, D. H., & Huang, L. H. (2012). Accurate solution to diffraction around a modified V-shaped breakwater. *Coastal engineering*, *68*, 56-66.

[48] Feynman, R. P., Leighton, R. B., & Sands, M. (2011). *The Feynman lectures on physics, Vol. I: The new millennium edition: mainly mechanics, radiation, and heat* (Vol. 1). Basic books.

[49] Chu, Y. C., Cheng, J. S., Wang, J. Q., Li, Z. G., & Jiang, K. B. (2014). Hydrodynamic performance of the arc-shaped bottom-mounted breakwater. *China Ocean Engineering*, 28(6), 749-760.

[50] Liu, J., & Lin, G. (2013). Scaled boundary FEM solution of short-crested wave interaction with a concentric structure with double-layer arc-shaped perforated cylinders. *Computers & Fluids*, *79*, 82-104.

[51] Liu, Y. (2019). HAMS: A Frequency-Domain Preprocessor for Wave-Structure Interactions—Theory, Development, and Application. *Journal of Marine Science and Engineering, 7*(3), 81.

[52] Liu, Y., Yoshida, S., Hu, C., Sueyoshi, M., Sun, L., Gao, J., Cong P. & He, G. (2018). A reliable open-source package for performance evaluation of floating renewable energy systems in coastal and offshore regions. *Energy conversion and management*, *174*, 516-536.

[53] Lee, C. H., & Newman, J. N. (1999). *WAMIT User manual*. Dept. of Ocean Engineering, Massachusetts Institute of Technology, Cambridge, MA.

[54] Plymouth coastal observatory. (2020). Live waves and tides. Retrieved from http://southwest.coastalmonitoring.org/live-waves-and-tides/.